ELSEVIER

Comput. Methods Appl. Mech. Engrg. 191 (2002) 2611–2630

Computer methods in applied mechanics and engineering

www.elsevier.com/locate/cma

On the optimal shape parameters of radial basis functions used for 2-D meshless methods

J.G. Wang [a,*], G.R. Liu [b]

[a] Department of Civil Engineering, Tropical Marine Science Institute, National University of Singapore, 10 Kent Ridge Crescent, Singapore 119260, Singapore

[b] Department of Mechanical and Production Engineering, Centre of Advanced Computations in Engineering Science, National University of Singapore, 10 Kent Ridge Crescent, Singapore 119260, Singapore

Received 30 March 2001; received in revised form 15 October 2001; accepted 23 November 2001

Abstract

A radial point interpolation meshless (or radial PIM) method was proposed by authors to overcome the possible singularity associated with only polynomial basis. The radial PIM used multiquadric (MQ) or Gaussian as basis functions. These two radial basis functions all included shape parameters. Although choice of shape parameters has been a hot topic in approximation theory and some empirical formulae were proposed, how these shape parameters affect the accuracy of the radial PIM has not been studied yet. This paper studied the effect of shape parameters on the numerical accuracy of radial PIM. A range of suitable shape parameters is obtained from the analysis of the condition number of the system matrix, error of energy and irregularity of node distribution. It is observed that the widely used shape parameters for MQ and reciprocal MQ basis are not even close to their optimums. The optimal shape parameters are found in this paper to be simply $q = 1.03$ and $R = 1.42$ for MQ basis and $c = 0.003$–0.03 for Gaussian basis.

Keywords: Meshless method; Radial basis function; Optimal shape parameters; Stress analysis

1. Introduction

Meshless methods have achieved remarkable progress in recent years. Main efforts have been focusing on different approximation methods over a cluster of scattered nodes. Radial point interpolation method (radial PIM) [1] is one of meshless methods. It was used to solve partial differential equations for solid mechanics over unstructured nodes. The radial PIM has several attractive features. First, its approximation function passes through each node point in the influence domain and thus has the interpolation with delta property. This property makes the implementation of essential boundary conditions much easier than the meshless methods based on the moving least-square methods such as element-free Galerkin (EFG) method [2]. Second, its shape functions and derivatives are easily developed only if basis functions and distributions

* Corresponding author.
E-mail address: tmswjg@nus.edu.sg (J.G. Wang).

0045-7825/02/$ - see front matter
PII: S0045-7825(01)00419-4

of nodes are determined. The widely used radial basis functions (rbfs) are multiquadric (MQ) [3] and Gaussian (EXP) [4]. They are true grid free schemes for approximating surfaces in an arbitrary number of dimensions. Third, the basis functions are continuously differentiable and integrable. This is useful for rbfs to solve differential equations. Finally, the exponential convergence rate of MQ [5] makes it superior to the EXP and other rbfs such as thin plate spline (TPS) [6].

Rbf has more than 30-year history, however the history to use rbf in solving partial differential equations (PDEs) is short. Kansa [7] was the pioneer who adopted radial basis functions to solve Navier–Stokes equations of fluid flow. He discretized the PDEs directly over unstructured nodes through MQ basis functions. His method was similar to finite difference method (FDM) but suitable for any scattered distribution of nodes. He found that the key factor in obtaining accurate results was the condition number of the MQ coefficient matrix. The condition number can be adjusted through variable shape parameters. Collocation methods were recently developed as a promising meshless method [8–12]. Collocation methods should be called as true meshless methods because they do not require any element for either interpolation or integration. The associated problem of full system matrix can be solved by introducing compactly supported basis functions [9,12]. However, collocation methods have two issues of demerits except numerical stability: The first issue is the treatment of boundary conditions including internal and external boundaries. Current treatments are almost the same methods as those used in FDM. Such treatments will destroy some properties of system stiffness matrix such as symmetry. The second issue is the requirement of higher derivatives of shape functions. Higher derivatives are sometimes difficult to be developed in practice, especially in the overlapping zone of compactly supported domains. This is because the lower smoothness always occurs in the center point and edge [9] of such a domain. Meshless methods based on weak forms such as radial PIM eliminate above disadvantages. The weak form requires lower order of derivatives in internal points and along boundary conditions. This makes the implementation of boundary conditions much easier. A disadvantage for such a meshless method is that background cell is required for integration.

The advantages of the meshless methods with rbfs are attractive, however there are two issues still to be solved: first, MQ and EXP are generally used as globally supported functions instead of local ones. Globally supported functions produce a full system matrix. A full system matrix is a headache problem due to ill-conditioning, memory requirement and computation efficiency. Some methods such as domain decomposition are employed to divide a big problem into many small quasi-local problems [7]. This decomposition can produce a sparse system matrix. Radial PIM [1] used compactly supported domain and produced a banded system matrix. Second, MQ and EXP basis functions involve shape parameters [1,12]. Our preliminary numerical study [1] indicates the shape parameters have important effect on the accuracy of the radial PIM. How the shape parameters affect the accuracy has not been studied yet.

The choice of shape parameters has been a hot topic in data fittings [13–16]. Franke [13] evaluated about 30 interpolation schemes in two dimensions and found that the most accurate two schemes were MQ and TPS. He suggested the shape parameter $R = 1.25D/\sqrt{N}$ in MQ basis. Where D is the diameter of the minimal circle enclosing all data points and N is the number of data points. Hardy [3] recommended $R = 0.815d$ where $d = (1/N)\sum_{i=1}^{N} d_i$ and d_i is the distance between the ith data point and its nearest neighbor. Rippa [14] proposed an algorithm for selecting a good value of shape parameter in MQ, inverse MQ and Gaussian interpolants. Carlson and Foley [15] obtained a result that the optimal shape parameter was most strongly influenced by the magnitude of function values, the number of data points. But their location in the domain has little influence. All above are working on the global data domain and only the accuracy of approximation is concerned. In the numerical solutions of PDEs, Golberg et al. [10,16] discussed the error analysis for the dual reciprocity method (DRM) with rbf approximation and boundary integral equations. They found that the convergence behavior of the DRM depends on both interpolation error and the error of boundary element method (BEM). They used a technology of cross validation to

optimize the shape parameter of MQ basis. That technology is based on statistical cross validation. Kansa [7] proposed a scheme that allows the shape parameter of MQ to vary with basis functions. He observed that the more distinct the entries of the MQ coefficient matrix are, the lower the MQ coefficient matrix condition number becomes, and the better the accuracy is. All of them just optimize a single shape parameter in rbfs.

However, the error of radial PIM comes from two sources: radial basis approximation and Galerkin weak form. This is because influence domain is local instead of global. The shape parameters have vital effect on the compactly supported property of influence domain. A general theoretical analysis on how the shape parameter is associated with the accuracy of approximation is difficult. Based on our previous paper [1], this paper will numerically and systemically study the effect of shape parameters of MQ and Gaussian basis functions on the accuracy of radial PIM. MQ here is a little different from the original MQ or reciprocal multiquadric (RMQ) where the shape parameter $q = 0.5$ or -0.5. This paper is organized as follows: In Section 2, we review the point interpolation by rbfs and Galerkin weak form of two-dimensional (2-D) solid mechanics problems. The shape parameters are introduced for MQ and EXP basis functions. In Section 3 the accuracy of approximation is evaluated through interpolation and condition number. Section 4 studies some numerical examples to find out the range of good shape parameters. Finally, the optimal shape parameters are recommended.

2. Outline of radial point interpolation meshless method

The radial PIM has two essential components: Interpolation through rbfs and Galerkin weak form. This section will briefly review the two components.

2.1. Radial point interpolation

Construct an interpolation of $u(\mathbf{x})$ to pass through all nodes using rbf $B_i(\mathbf{x})$ and polynomial basis function $p_j(\mathbf{x})$ as follows:

$$u(\mathbf{x}) = \sum_{i=1}^{n} B_i(\mathbf{x}) a_i + \sum_{j=1}^{m} P_j(\mathbf{x}) b_j = \mathbf{B}^{\mathrm{T}}(\mathbf{x})\mathbf{a} + \mathbf{P}^{\mathrm{T}}(\mathbf{x})\mathbf{b} \tag{1}$$

where a_i is the coefficient for $B_i(\mathbf{x})$ and b_j is the coefficient for $p_i(\mathbf{x})$, n is the number of nodes in an influence domain of $\mathbf{x}$, m is the polynomial term which is usually $m < n$. The vectors are defined as

$$\begin{aligned} &\mathbf{a} = [a_1, a_2, a_3, \ldots, a_n]^{\mathrm{T}}, \\ &\mathbf{b} = [b_1, b_2, \ldots, b_m]^{\mathrm{T}}, \\ &\mathbf{B}^{\mathrm{T}}(\mathbf{x}) = [B_1(\mathbf{x}), B_2(\mathbf{x}), B_3(\mathbf{x}), \ldots, B_n(\mathbf{x})], \\ &\mathbf{P}^{\mathrm{T}}(\mathbf{x}) = [p_1(\mathbf{x}), p_2(\mathbf{x}), \ldots, p_m(\mathbf{x})]. \end{aligned} \tag{2}$$

Radial basis is a function of distance r_i defined as follows:

$$\begin{aligned} &B_i(\mathbf{x}) = B_i(r_i), \\ &r_i = \left[(x - x_i)^2 + (y - y_i)^2\right]^{1/2}. \end{aligned} \tag{3}$$

Polynomial basis has following monomial terms:

$$\mathbf{P}^{\mathrm{T}}(\mathbf{x}) = [1, x, y, x^2, xy, y^2, \ldots]. \tag{4}$$

Enforcing the interpolation pass through all n scattered points within the influence domain, a set of equations on the coefficients a_i and b_j is setup:

$$u_k = u(x_k, y_k) = \sum_{i=1}^{n} a_i B_i(x_k, y_k) + \sum_{j=1}^{m} b_j P_j(x_k, y_k), \quad k = 1, 2, \ldots, n. \tag{5}$$

The radial term transforms a multidimension into one-dimension, and the polynomial term improves the polynomial accuracy of the interpolation. As commented in [4] and our research [1], addition of polynomial terms does not improve greatly the accuracy for non-polynomial functions. But theoretical study [17] revealed that there was no guarantee that the interpolating condition could be satisfied without the addition of polynomial terms. Furthermore, the coefficients should be constrained so that the interpolation is unique [18]. Following constraints are usually imposed:

$$\sum_{i=1}^{n} P_j(x_i, y_i) a_i = 0, \quad j = 1, 2, \ldots, m. \tag{6}$$

Eqs. (5) and (6) are expressed in matrix form as follows:

$$\begin{bmatrix} \mathbf{B}_0 & \mathbf{P}_0 \\ \mathbf{P}_0^{\mathrm{T}} & \mathbf{0} \end{bmatrix} \begin{Bmatrix} \mathbf{a} \\ \mathbf{b} \end{Bmatrix} = \begin{Bmatrix} \mathbf{u}^e \\ \mathbf{0} \end{Bmatrix} \quad \text{or} \quad \mathbf{G} \begin{Bmatrix} \mathbf{a} \\ \mathbf{b} \end{Bmatrix} = \begin{Bmatrix} \mathbf{u}^e \\ \mathbf{0} \end{Bmatrix} \tag{7}$$

where the vector of function values at each node is

$$\mathbf{u}^e = [u_1, u_2, u_3, \ldots, u_n]^{\mathrm{T}}. \tag{8}$$

The coefficient matrix $\mathbf{B}_0$ on unknowns $\mathbf{a}$ is

$$\mathbf{B}_0 = \begin{bmatrix} B_1(x_1, y_1) & B_2(x_1, y_1) & \cdots & B_n(x_1, y_1) \\ B_1(x_2, y_2) & B_2(x_2, y_2) & \cdots & B_n(x_2, y_2) \\ \vdots & \vdots & \vdots & \vdots \\ B_1(x_n, y_n) & B_2(x_n, y_n) & \cdots & B_n(x_n, y_n) \end{bmatrix}_{n \times n}. \tag{9}$$

The coefficient matrix $\mathbf{P}_0$ on unknowns $\mathbf{b}$ is

$$\mathbf{P}_0 = \begin{bmatrix} P_1(x_1, y_1) & P_2(x_1, y_1) & \cdots & P_m(x_1, y_1) \\ P_1(x_2, y_2) & P_2(x_2, y_2) & \cdots & P_m(x_2, y_2) \\ \vdots & \vdots & \vdots & \vdots \\ P_1(x_n, y_n) & P_2(x_n, y_n) & \cdots & P_m(x_n, y_n) \end{bmatrix}_{n \times m}. \tag{10}$$

The distance is directionless, $B_k(x_i, y_i) = B_i(x_k, y_k)$. Unique solution is obtained if the inverse of matrix $\mathbf{G}$ exists:

$$\begin{Bmatrix} \mathbf{a} \\ \mathbf{b} \end{Bmatrix} = \mathbf{G}^{-1} \begin{Bmatrix} \mathbf{u}^e \\ 0 \end{Bmatrix}. \tag{11}$$

And the interpolation is expressed as

$$u(\mathbf{x}) = \left[\mathbf{B}^{\mathrm{T}}(\mathbf{x}) \mathbf{P}^{\mathrm{T}}(\mathbf{x})\right] \mathbf{G}^{-1} \begin{Bmatrix} \mathbf{u}^e \\ \mathbf{0} \end{Bmatrix} = \boldsymbol{\varphi}(\mathbf{x}) \mathbf{u}^e \tag{12}$$

where the matrix of shape functions $\boldsymbol{\varphi}(\mathbf{x})$ is defined as

$$\boldsymbol{\varphi}(\mathbf{x}) = [\phi_1(\mathbf{x}), \phi_2(\mathbf{x}), \ldots, \phi_i(\mathbf{x}), \ldots, \phi_n(\mathbf{x})] \tag{13}$$

in which

$$\phi_k(\mathbf{x}) = \sum_{i=1}^{n} B_i(\mathbf{x})\overline{G}_{i,k} + \sum_{j=1}^{m} P_j(\mathbf{x})\overline{G}_{n+j,k} \tag{14}$$

where $\overline{G}_{i,k}$ is the (i,k) element of matrix $\mathbf{G}^{-1}$. The derivatives of shape functions are

$$\begin{aligned} \frac{\partial \phi_k}{\partial x} &= \sum_{i=1}^{n} \frac{\partial B_i}{\partial x}\overline{G}_{i,k} + \sum_{j=1}^{m} \frac{\partial P_j}{\partial x}\overline{G}_{n+j,k}, \\ \frac{\partial \phi_k}{\partial y} &= \sum_{i=1}^{n} \frac{\partial B_i}{\partial y}\overline{G}_{i,k} + \sum_{j=1}^{m} \frac{\partial P_j}{\partial y}\overline{G}_{n+j,k}. \end{aligned} \tag{15}$$

The original form of multiquadric is extended to following form [1] (called MQ, too):

$$B_i(x,y) = \left(r_i^2 + R^2\right)^q, \quad R \geqslant 0. \tag{16}$$

Its partial derivatives are easily obtained as follows:

$$\begin{aligned} \frac{\partial B_i}{\partial x} &= 2q\left(r_i^2 + R^2\right)^{q-1}(x - x_i), \\ \frac{\partial B_i}{\partial y} &= 2q\left(r_i^2 + R^2\right)^{q-1}(y - y_i) \end{aligned} \tag{17}$$

where q and R are shape parameters. When $q = 0.5$, Eq. (16) becomes the original MQ [3]. When $q = -0.5$, it reduces to the RMQ [3].

Gaussian form (called EXP) has been widely studied by mathematicians [19–21]:

$$B_i(x,y) = \exp\left(-c\left(\frac{r_i}{r_{\max}}\right)^2\right) \tag{18}$$

where c $(c \geqslant 0)$ is a shape parameter. $r_{\max}$ is the maximum distance of neighborhood nodes in the influence domain. Its partial derivatives are again obtained as follows:

$$\begin{aligned} \frac{\partial B_i}{\partial x} &= -\frac{2c}{r_{\max}^2} B_i(x,y)(x - x_i), \\ \frac{\partial B_i}{\partial y} &= -\frac{2c}{r_{\max}^2} B_i(x,y)(y - y_i). \end{aligned} \tag{19}$$

2.2. Galerkin weak form of 2-D solid mechanics problem

A 2-D problem of solid mechanics can be described by equilibrium equation in domain Ω bounded by Γ $(\Gamma = \Gamma_t + \Gamma_u)$:

$$\nabla \cdot \boldsymbol{\sigma} + \mathbf{F} = 0 \quad \text{in } \Omega \tag{20}$$

where $\boldsymbol{\sigma}$ is the stress tensor and $\mathbf{F}$ the body force vector. Boundary conditions are given as follows:

$$\begin{aligned} &\boldsymbol{\sigma} \cdot \mathbf{n} = \bar{\mathbf{t}} \quad \text{on the natural boundary } \Gamma_t, \\ &\mathbf{u} = \bar{\mathbf{u}} \quad \text{on the essential bounary } \Gamma_u \end{aligned} \tag{21}$$

where the superposed bar denotes prescribed boundary values and **n** is the unit outward normal to the domain. Its weak form is expressed as

$$\int_{\Omega} \delta(\nabla_s \mathbf{u}^{\mathrm{T}}) \cdot \boldsymbol{\sigma} \, \mathrm{d}\Omega - \int_{\Omega} \delta \mathbf{u}^{\mathrm{T}} \cdot \mathbf{F} \, \mathrm{d}\Omega - \int_{\Gamma_t} \delta \mathbf{u}^{\mathrm{T}} \cdot \bar{\mathbf{t}} \, \mathrm{d}\Gamma = 0. \tag{22}$$

Discretization of Eq. (22) with Eq. (12) yields

$$\mathbf{K}\mathbf{u} = \mathbf{f} \tag{23}$$

where

$$\mathbf{K}_{ij} = \int_{\Omega} B_i^{\mathrm{T}} D B_j \, \mathrm{d}\Omega, \qquad f_i = \int_{\Gamma_t} \phi_i \bar{\mathbf{t}} \, \mathrm{d}\Gamma + \int_{\Omega} \phi_i \mathbf{F} \, \mathrm{d}\Omega. \tag{24}$$

For plane (stress) problem

$$\begin{aligned} B_i &= \begin{bmatrix} \phi_{i,x} & 0 \\ 0 & \phi_{i,y} \\ \phi_{i,y} & \phi_{i,x} \end{bmatrix}, \\ \mathbf{D} &= \frac{E}{1-v^2} \begin{bmatrix} 1 & v & 0 \\ v & 1 & 0 \\ 0 & 0 & (1-v)/2 \end{bmatrix}. \end{aligned} \tag{25}$$

The numerical procedure is listed as follows:

1. Loop over background cells to determine all Gauss points to find out its location and weight. Remove the background cells.
2. Loop over Gauss points for integration of Eq. (24)
   a. Determine the domain of influence for specified Gauss point and select neighboring nodes based on a defined criterion;
   b. Compute shape function and its derivatives for each Gauss point;
   c. Evaluate stiffness and load at each Gauss point;
   d. Assemble the contribution of each Gauss point to form system equation;
3. Introduce essential and load boundaries.
4. Solve the system equation to obtain nodal displacements.
5. Evaluate strain and stress at each Gauss point.

3. Error function for evaluation

3.1. Shape function and condition number

As discussed in Section 1, errors of the radial PIM are from two sources: interpolation of rbfs and the Galerkin weak form. This section will only discuss the relationship of interpolation accuracy and the condition number. First of all, let us see how the shape parameters affect shape functions. This discussion here does not include polynomial term in the basis functions ($m = 0$).

Fig. 1 gives the shape functions (1-D case) of for MQ and EXP basis functions with different shape parameters, respectively. For EXP basis, when the c is larger, because exponential function decays more

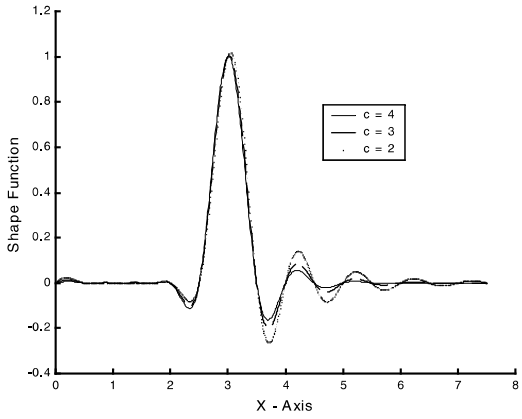

(a) Effect of shape parameter c on shape functions (EXP basis)

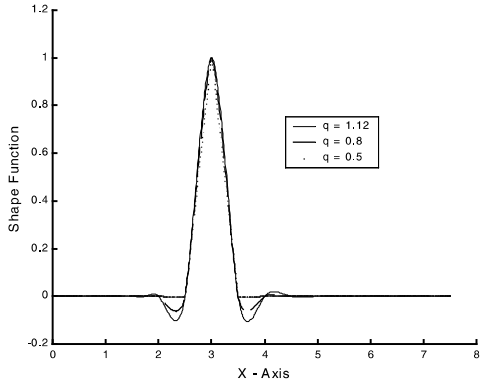

(b) Effect of shape parameter q on shape functions (MQ basis)

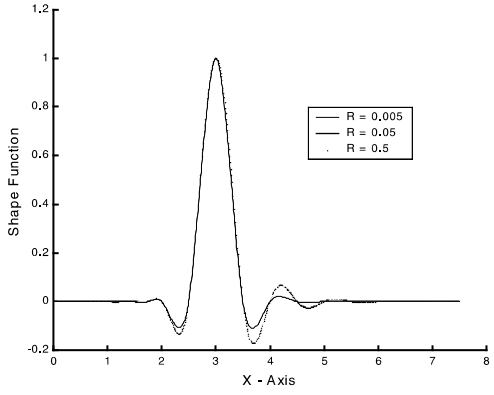

(c) Effect of shape parameter R on shape functions (MQ basis)

Fig. 1. Effect of shape parameters on shape functions.

quickly, the smaller influence domain of shape functions is. When the c is less than 1.0, shape functions oscillates from their two wings. This may be due to the interfering of influence domains. The MQ basis has a shape function without oscillation for any shape parameter. When the shape parameters q and R are bigger, shape functions have wider wings. As a summary, the MQ basis has a shape function without

oscillation while the EXP has a shape function which is oscillatory or not heavily depended on its shape parameter.

Above properties of interpolation are associated with the condition number of matrix. The condition number of matrix is an important factor to affect the numerical results of the radial point interpolation. Here we will study the relationship between condition number and interpolation accuracy (use $f = \sin(x)\cos(y)$ as an example). Five sets of node patterns are randomly generated within the domain of $[0,1]\times[0,1]$ to determine the shape functions. Then this domain is subdivided into regular grids with an increment of 0.1 to form an evaluation grid. At each grid node true function and interpolation through above radial point interpolation are evaluated. The norm of errors at all grid nodes (called function error) is obtained through their comparison.

Fig. 2 gives the effect of shape parameters on condition number and accuracy for EXP basis. The condition number almost linearly decreases with the shape parameter c. Different node distribution patterns have a little effect, too. Generally, condition number ranges within 10^2–10^4 order for different node distributions and same shape parameter. When the shape parameter is smaller than 10^{-3} (or smallest value), the condition number approaches to infinite (here "infinite" refers to the limit of computer precision). The accuracy is lower when the shape parameter is larger than some critical value, although the condition number is lower in this zone. The accuracy varies little when the shape parameter is smaller than the critical value. As we know, large condition number means that the matrix is ill-conditioned and its inversion will cause bigger error. Therefore, the shape parameter should be not too small. There should be an optimal value between the smallest value and the critical value.

The MQ basis has a little different property for condition number and interpolation accuracy as shown in Fig. 3. First, the matrix is singular when q equals to integer such as $1, 2, \ldots$ Matrices $\mathbf{B}_0$ and $\mathbf{G}$ have almost the same types of condition numbers. Second, condition number changes little with shape parameter q except around 1 and is much lower except singular cases. Third, the shape parameter R has vital effect on the condition number. When R changes from 0.1 to 2.0, the condition number increases around 10^5 order. Fourth, interpolation accuracy is almost the same for $q < 1$ and each R. The accuracy increases sharply when the q is around 1.0. From the view of accuracy, the bigger R is better.

As a conclusion, whether the rbfs are the MQ or EXP, the condition number of matrix and accuracy of interpolation heavily depend on shape parameters. Node distribution has a little effect. There exist optimal shape parameters for MQ and EXP basis functions, probably the optimal shape parameters should be $q \approx 1.0$ and $R = 1.5$–2.0 for MQ basis and $c < 0.5$ for EXP basis.

3.2. Error index for radial PIM

For a boundary-value problem, the error can be spilt into two components: the one due to the Galerkin weak form and the other due to approximation of real functions within an influence domain. Of course, the weak form and interpolation are also important to the convergence rate of the radial PIM. Unfortunately, we are unaware of any complete convergence analysis except some numerical results [1,4,10,11,15,17]. Therefore, the evaluation index for radial PIM should be different from those used only for approximation over scattered data. A relative error of displacements is defined as follows:

$$\delta = \frac{\sum_{i=1}^{n} \left| u_i^{\text{Exact}} - u_i^{\text{PIM}} \right|}{\sum_{i=1}^{n} \left| u_i^{\text{Exact}} \right|} \times 100\ (\%). \tag{26}$$

Alternatively, an error of energy can comprehensively understand the convergence rate:

$$e_e = \frac{1}{2LD} \left\{ \int_{\Omega} (\varepsilon^{\text{PIM}} - \varepsilon^{\text{Exact}})^{\text{T}} : (\sigma^{\text{PIM}} - \sigma^{\text{Exact}})\, \mathrm{d}\Omega \right\}^{1/2} \tag{27}$$

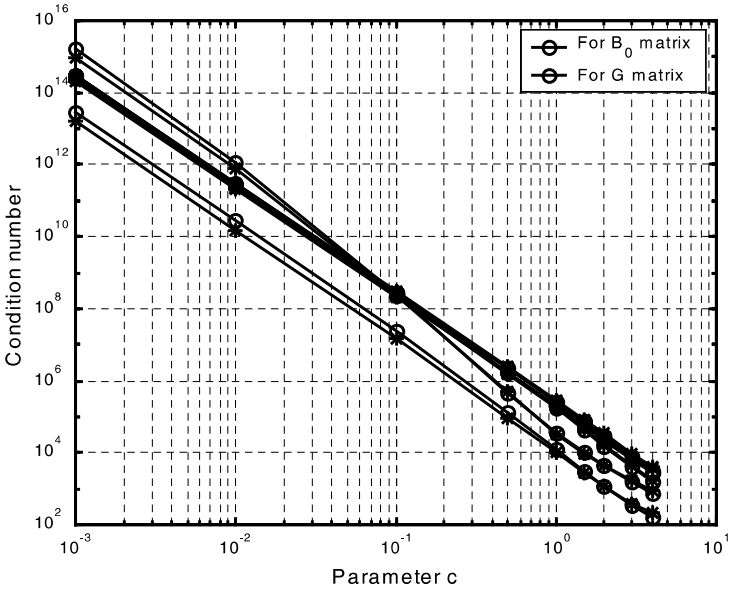

(a) Variation of condition number with node distributions

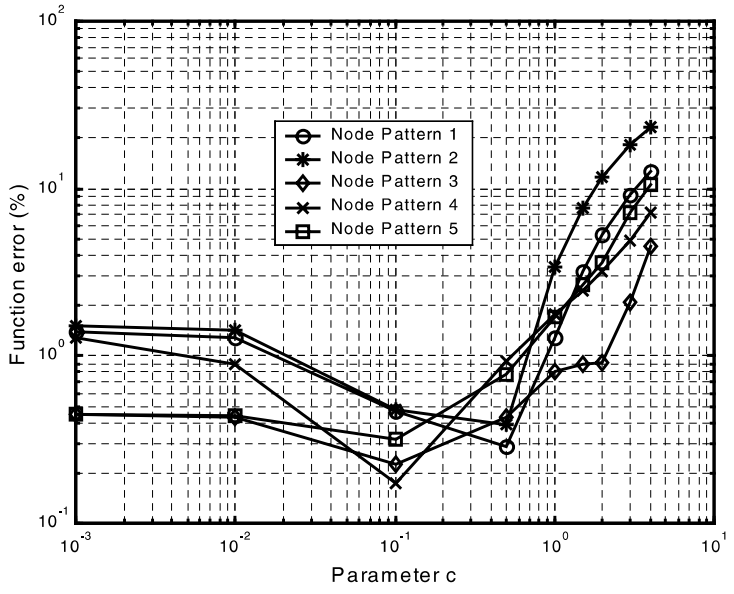

(b) Variation of interpolation accuracy with node distributions

Fig. 2. Effect of shape parameters on condition number and accuracy for EXP basis.

where u_i^{PIM} and u_i^{Exact} are displacements computed by the radial PIM and closed-form solution, respectively. $\varepsilon^{\mathrm{PIM}}$ and σ^{PIM} are strain and stress tensors obtained from the radial PIM. The superscript 'Exact' refers to the components obtained by closed-form solutions.

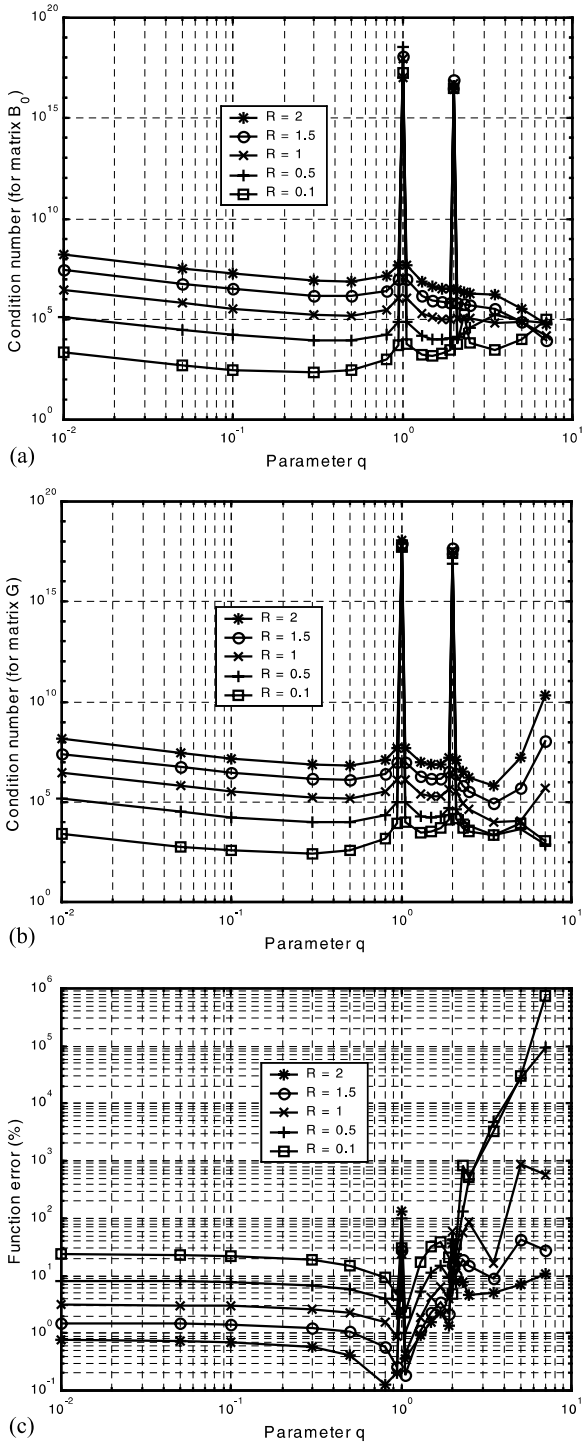

Fig. 3. Effect of shape parameters on condition number and accuracy for MQ basis.

4. Numerical experiments of 2-D solid mechanics problems

4.1. Cantilever beam

4.1.1. Closed-form solution

A cantilever beam problem as shown in Fig. 4 is studied. The beam has a unit thickness and hence a plane stress problem is assumed. The closed-form solution is available for parabolic traction of force P [22]:

$$\begin{aligned} u_x &= \frac{Py}{6EI}\left[(6L-3x)x+(2+v)\left(y^2-\frac{D^2}{4}\right)\right], \\ u_y &= -\frac{P}{6EI}\left[3vy^2(L-x)+(4+5v)\frac{D^2x}{4}+(3L-x)x^2\right] \end{aligned} \tag{28}$$

where the moment of inertia I of the beam is given $I = D^3/12$.

The corresponding stresses are

$$\sigma_x = \frac{P(L-x)y}{I}, \qquad \tau_{xy} = -\frac{P}{2I}\left[\frac{D^2}{4}-y^2\right], \qquad \sigma_y = 0 \tag{29}$$

The beam parameters are taken as $E = 3.0 \times 10^7$ kPa, $v = 0.3$, $D = 12$ m, $L = 48$ m and $P = 1000$ kN in the computation.

4.1.2. Effect of shape parameters for regular node distribution

A regular node distribution (637 nodes) as shown in Fig. 4(b) is used to study the effect of shape parameters. The radius of influence domain is fixed as

$$d_{\max} = C_I \times h \tag{30}$$

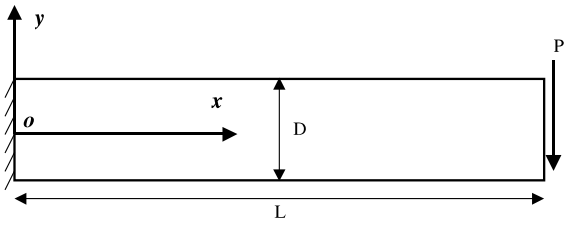

(a) Cantilever beam problem

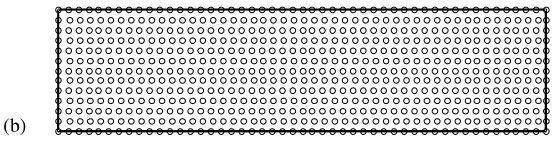

(b)

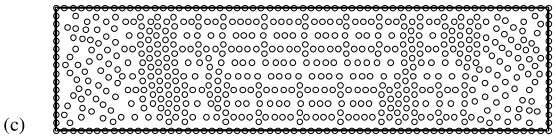

(c)

Fig. 4. Cantilever beam problem and its meshless models.

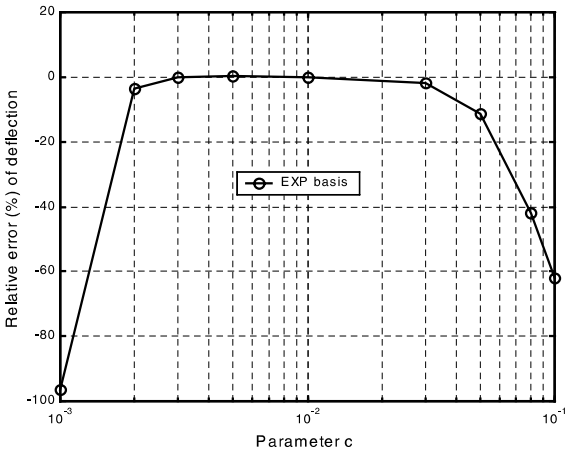

(a) Relative error for EXP basis

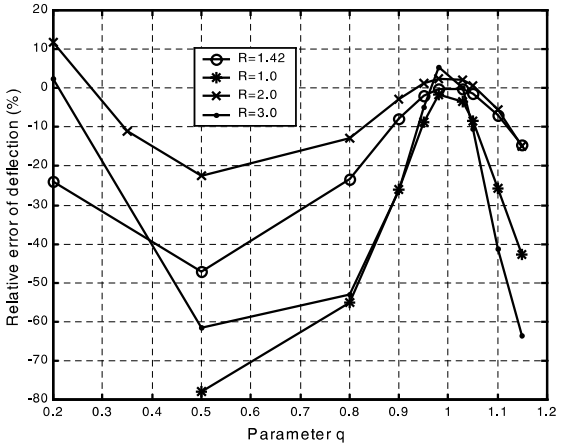

(b) Relative error for MQ basis

Fig. 5. Shape parameter effect on relative error of maximum deflection.

Here the coefficient is fixed as $C_I = 2.0$ in the present computation, and h is the maximum distance among neighboring nodes of the influence domain (for this case $h = r_{\max} = 1.0$). Square influence domain circumvents 9–16 nodes for each Gaussian point. Polynomial term is not included for the time beings ($m = 0$).

Fig. 5 gives the variation of relative errors of deflection with shape parameters. The EXP basis is not sensitive when $c = 0.002$–0.03. However, the MQ basis performs a little sensitively to the shape parameters of q and R. The same phenomenon is observed for the error of energy as shown in Fig. 6. The optimal shape parameter q is around 1. In order to observe the local variation near the optimum, Figs. 7 and 8 give the local view in the zone of $q = [0.9, 1.06]$ on the relative error of deflection and error of energy. From these figures, we can understand following properties of MQ basis: First, when $q = 0.5$, which is the original multiquadric basis [3], the relative error is not acceptable for the present shape parameter R. The accuracy is the most sensitive to the shape parameter R. Although a best accuracy can be achieved through shape parameter R, this is the case many researchers have been studying [7–16], the best accuracy is still far away from the optimum. Second, the minimum relative error of deflection and error of energy are achieved when

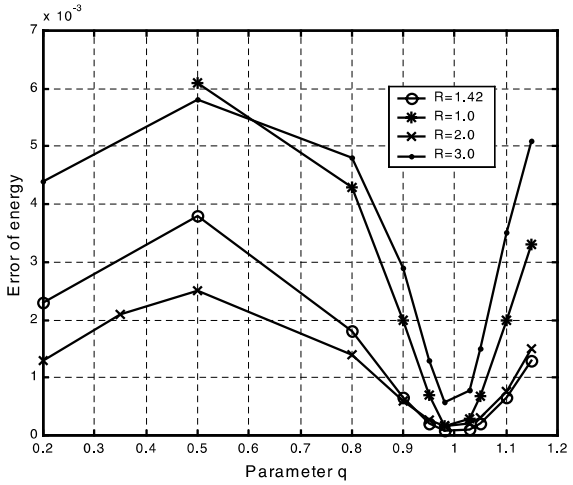

Fig. 6. Optimal shape parameters for MQ basis.

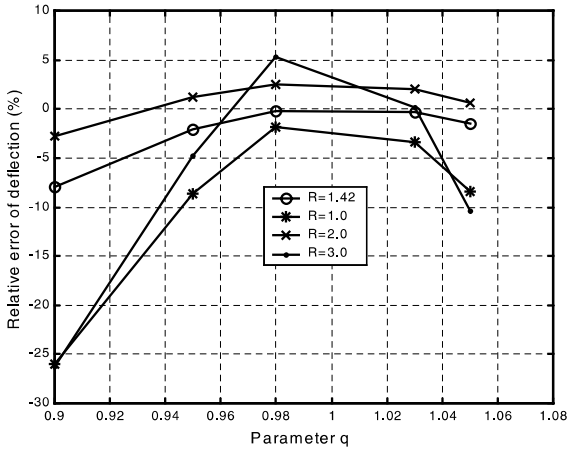

Fig. 7. Local view of relative error of deflection around shape parameter $q = 1.0$.

$q = 0.98$–1.03 regardless of shape parameter R. This implies that the optimal shape parameter q is almost independent of shape parameter R. The $q = 1.03$ can be regarded as an optimum of this problem. Third, the shape parameter R has little effect on the accuracy when $q = 1.03$. At the $q = 1.03$, the effect of the shape parameter R is shown in Fig. 9 for the error of energy. The optimal R is around 1.42. Fourth, the above optimal shape parameters also cover the range of $q < 0$. Fig. 10 is the relative error of deflection and error of energy for the negative q. The errors do not approach to an optimum within these zones. That is, there is no optimum in the negative q. Therefore, $q = -0.5$ is not an optimal shape parameter.

4.1.3. Effect of irregular node distributions

As an example, the node distribution shown in Fig. 4(c) is analyzed here. The model has approximately 637 nodes. The comparison of the energy error with regular node distribution is shown in Fig. 11. For EXP basis, node distributions affect the highest accuracy, however, the optimal range of shape parameter c is

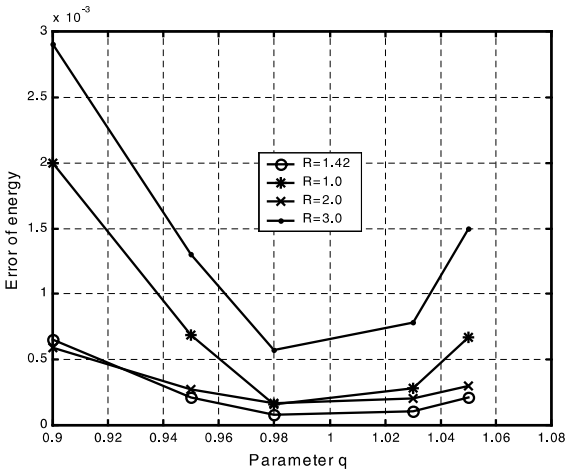

Fig. 8. Local view of error of energy around shape parameter $q = 1.0$.

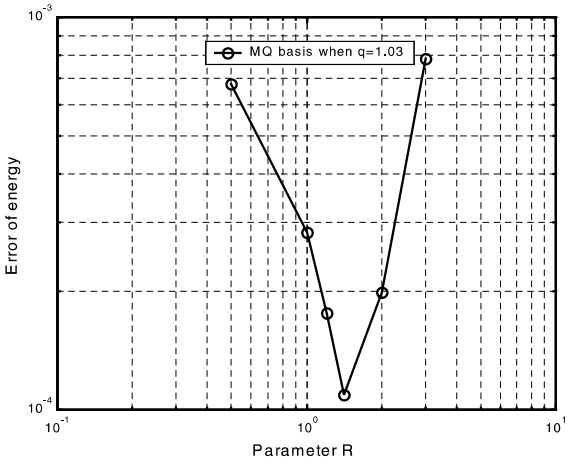

Fig. 9. Optimal R for fixed shape parameter ($q = 1.03$).

almost unchangeable. Both node distributions achieve acceptable accuracy within the same range of shape parameter. For MQ basis, the effect of shape parameter for irregular node distribution is similar to that of regular node distribution. That is, the energy error reaches its minimum when $q = [0.98, 1.03]$, and $q = 1.03$ and $R = 1.42$ reaches good accuracy. When $q = 0.5$ the accuracy heavily depends on the shape parameter R and the accuracy is much lower than the optimum. Therefore, $q = 0.5$ is not a suitable shape parameter for the radial PIM.

4.1.4. Effect of node density

This section checks whether above optimal shape parameters are suitable for different node densities or not. Fig. 12(a) plots the normalized shape parameter c (for EXP basis) against the error of energy. Each density has a range of shape parameters in which the error of energy almost keeps lowest. This range of shape parameters may slightly vary with node distribution patterns. This figure shows that the range of the

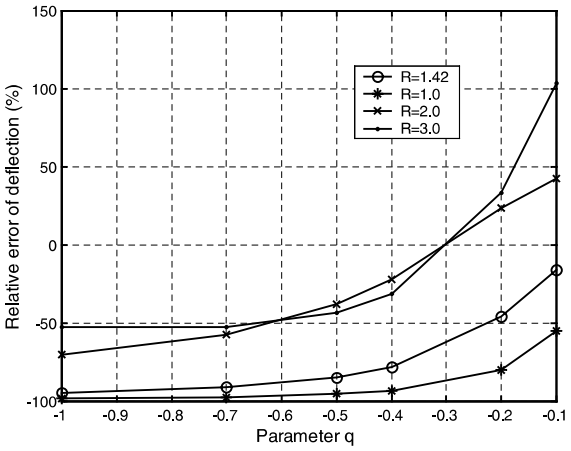

(a) Relative error of beam deflection at the free end

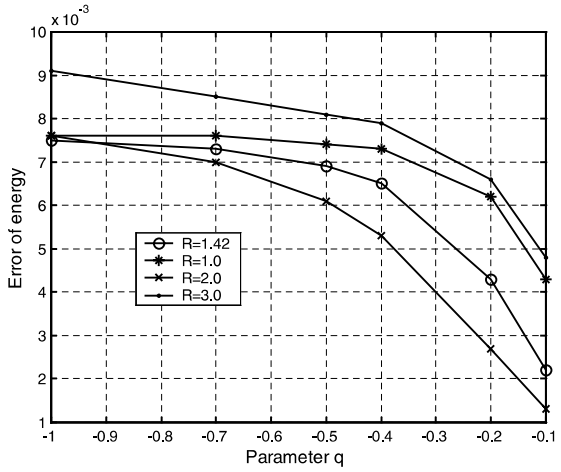

(b) Energy error of the cantilever beam

Fig. 10. Error analysis for the negative shape parameter q for MQ basis.

shape parameter c is 0.002–0.03 for 637 and 175 node cases. The 795-node case has a little narrower range. However, the optimal shape parameters for MQ basis do not change as shown in Fig. 12(b). In the computation, the shape parameter R is fixed to 1.42. The optimal shape parameter is in $q = [0.98, 1.03]$ regardless of node density. In this range, the error of energy reaches the lowest and is almost the same for three node densities.

4.2. Perforated strip plate

This section will study a perforated strip plate problem. A plate with a central circular hole is subjected to a unidirectional tensile load of 1.0 in the x direction. Only quarter of the plate is simulated due to symmetry. The node distribution (209 nodes) is shown in Fig. 13. This is a typical plane stress problem. Material properties are $E = 3.0 \times 10^3$ kPa and $v = 0.3$. Symmetry conditions are imposed on the left and bottom edges. Hole surface is traction free. The closed-form solution of stresses [22] is as follows:

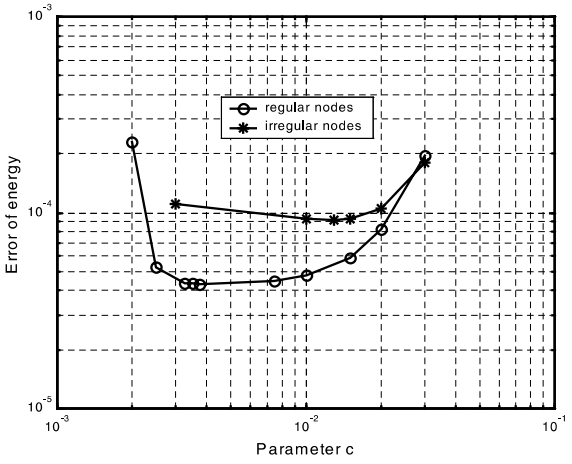

(a) For EXP basis

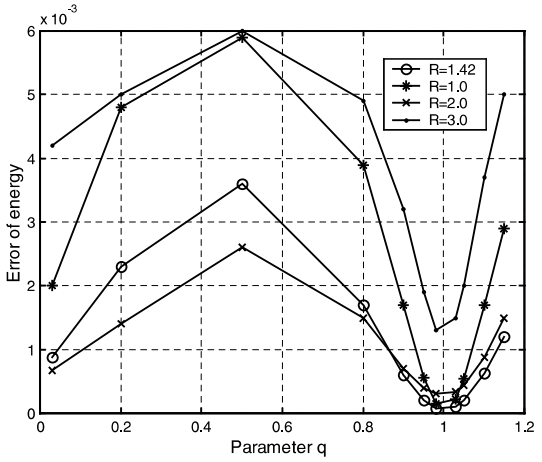

(b) For MQ basis (irregular node distribution)

Fig. 11. Effect of node distributions on the error of energy.

$$\begin{aligned}
\sigma_x(x,y) &= 1 - \frac{a^2}{r^2}\left\{\tfrac{3}{2}\cos 2\theta + \cos 4\theta\right\} + \frac{3a^4}{2r^4}\cos 4\theta,\\
\sigma_y(x,y) &= -\frac{a^2}{r^2}\left\{\tfrac{1}{2}\cos 2\theta - \cos 4\theta\right\} - \frac{3a^4}{2r^4}\cos 4\theta,\\
\sigma_{xy}(x,y) &= -\frac{a^2}{r^2}\left\{\tfrac{1}{2}\sin 2\theta + \sin 4\theta\right\} + \frac{3a^4}{2r^4}\sin 4\theta
\end{aligned} \tag{31}$$

where (r,θ) are polar coordinates. θ is measured counter-clockwise from the positive x-axis. a is the radius of the hole. For convenience, uniform traction is imposed on the right ($x = 50$) edge. For such a problem, the MQ basis is used to find the optimal shape parameters. Fig. 14 gives the error of energy with shape parameters and Fig. 15 gives the local view. The shape parameters of $q = 1.03$ and $R = 1.42$ are still suitable for this problem. The optimal shape parameter is almost the same as cantilever beam. It is noted that good

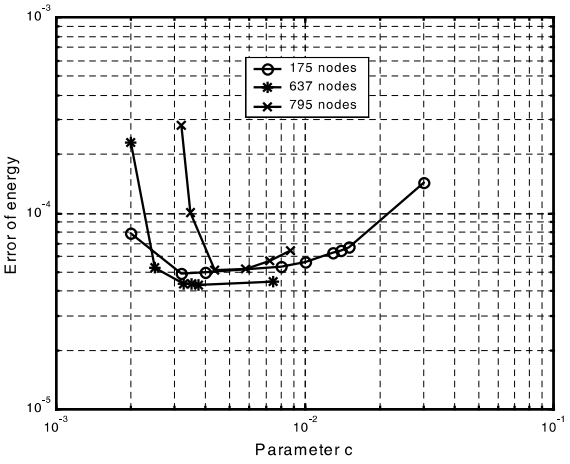

(a) For EXP basis

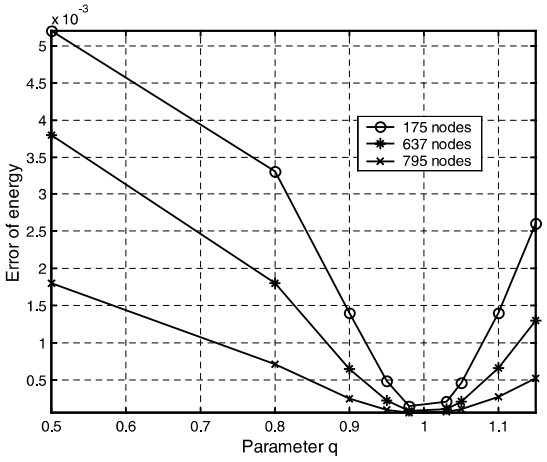

(b) For MQ basis ($R = 1.42$)

Fig. 12. Error of energy for different node densities.

shape parameters may not be unique. Fig. 14 indicates that the optimal shape parameter may have multiple choices, but the $q = 0.5$ is not an optimum. The EXP basis has similar results as $c = 0.003$–0.03.

4.3. Effect of polynomial terms

Above numerical analysis assumed that there was no polynomial term ($m = 0$) in the interpolation. This section will study the effect of polynomial terms. Only linear terms ($m = 3$) will be studied here. Table 1 compares the results of different problems under different node density. For the cantilever beam problem, the error of energy can reach 6.0×10^{-5} with a linear polynomial while the energy error without the polynomial term can only reach 1.39×10^{-4}. Linear polynomial terms can increase the accuracy of one order. Similar results are obtained for the perforated plate problem. For the interpolation with linear polynomial terms, energy error is not sensitive to the shape parameter q any more for the two examples. The accuracy reaches to almost the best.

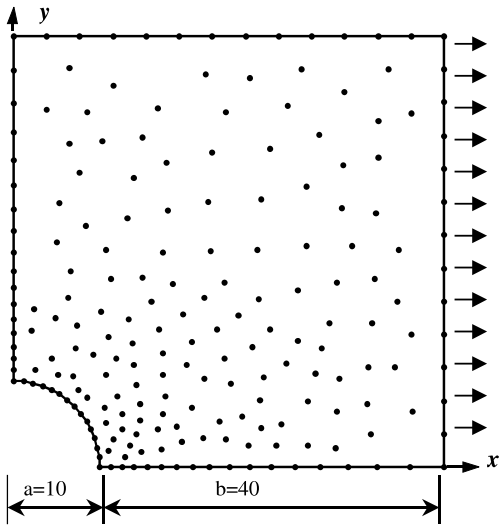

Fig. 13. Node distribution in perforated strip plate problem (subjected to tensile load in the x direction).

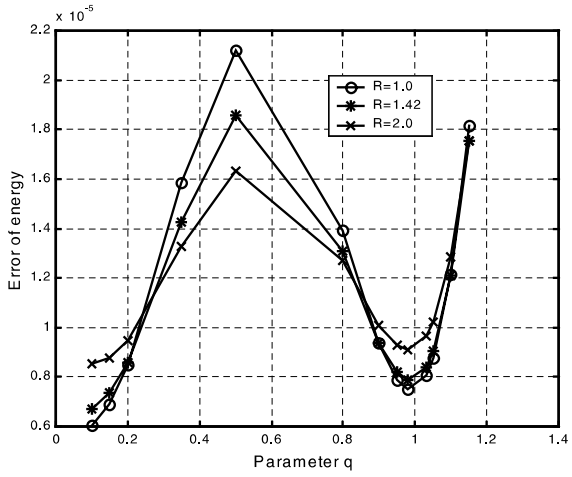

Fig. 14. Optimal shape parameters for perforated strip problem (MQ basis).

5. Conclusions

This paper studied the optimal shape parameters of MQ and Gaussian (EXP) basis for the 2-D radial PIM. The accuracy of data fitting depends only on interpolation, while the accuracy of the radial PIM depends on two components: (1) interpolation. (2) Galerkin weak form. Error of energy and relative error of deflection are defined as an error index in this paper. Two examples (2-D solid mechanics problems) were studied using such an index. The study can draw following conclusions:

(1) Radial basis interpolation is important to the global accuracy of the radial PIM. It is found that the condition number of the matrix $\mathbf{B}_0$ or $\mathbf{G}$ heavily affects the accuracy of interpolation. Shape parameters have vital effects on the condition number. For EXP basis, the condition number varies almost linearly with

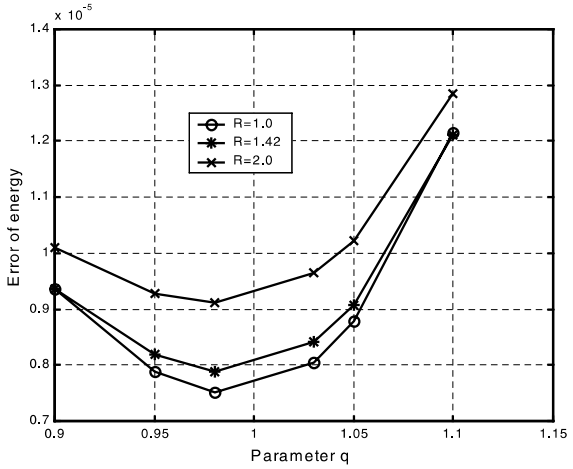

Fig. 15. Local view at $q = 1.0$ neighborhood for perforated strip plate problem.

Table 1
Comparison of energy error (MQ basis)

q ($R = 1.42$)	Cantilever beam				Perforated plate (209 nodes)	
	175 nodes		795 nodes		$m = 0$	$m = 3$
	$m = 0$	$m = 3$	$m = 0$	$m = 3$		
1.15	2.60E−3	6.05E−5	5.18E−4	4.49E−5	1.75E−5	7.39E−6
1.10	1.40E−3	6.12E−5	2.65E−4	4.46E−5	1.21E−5	7.31E−6
1.05	4.53E−4	6.18E−5	1.03E−4	4.43E−5	9.07E−6	7.23E−6
1.03	**2.02E−4**	6.21E−5	**6.81E−5**	4.42E−5	**8.42E−6**	7.21E−6
0.98	**1.39E−4**	6.29E−5	**5.69E−5**	4.39E−5	**7.89E−6**	7.14E−6
0.95	4.81E−4	6.33E−5	1.00E−4	4.38E−5	8.18E−6	7.11E−6
0.9	1.40E−3	6.40E−5	2.47E−4	4.35E−5	9.37E−6	7.06E−6
0.8	3.30E−3	6.55E−5	7.10E−4	4.30E−5	1.31E−5	6.96E−6
0.5	5.20E−3	6.88E−5	1.80E−3	4.20E−5	1.86E−5	6.77E−6

shape parameter c. The bigger the shape parameter, the smaller the condition number is. Node distribution can increase or decrease the condition number by 10^2–10^4 order. On the other hand, the smaller the shape parameter c, the higher the accuracy of interpolation is. A range of good shape parameters should balance the accuracy and the condition number. For MQ basis, the condition number is almost stable when $q < 1$. The higher the R, the bigger condition number is. When R varies from 0.1 to 2.0, the condition number increases around 10^5 order. When q is taken as integers, the matrix is almost singular. Furthermore, when q is around 1.0, the accuracy reaches the highest regardless of shape parameter R. When $q = 0.5$, the accuracy of MQ basis is the most sensitive to the shape parameter R.

(2) Numerical examples have revealed that good shape parameter c for EXP basis is 0.003–0.03. This range is valid for different node distributions and problems. Irregular node distribution will affect the highest accuracy but has little effect on the range of good shape parameter. Optimal shape parameters for MQ basis are $q = 1.03$ and $R = 1.42$ for cantilever beam and perforated strip plate. These two parameters are independent of node density, node distribution and problems. The original multiquadric where $q = 0.5$ and RMQ where $q = -0.5$ are not optimal shape parameters of the radial PIM. The accuracy at the

$q = \pm 0.5$ is sensitive to the shape parameter R and cannot reach the optimum regardless of R. This is the most significant result in this paper.

(3) The polynomial terms in Eq. (1) have vital effect on the accuracy of the radial PIM. Only linear polynomial basis is included in the computation, the energy accuracy can reduce one order. Furthermore, the results are almost the same over a range of shape parameters.

References

[1] J.G. Wang, G.R. Liu, A point interpolation meshless method based on radial basis functions, International Journal for Numerical Methods in Engineering, in press.
[2] T. Belytschko, Y. Krongauz, D. Organ, M. Fleming, P. Krysl, Meshless methods: an overview and recent developments, Computer Methods in Applied Mechanics and Engineering 139 (1996) 3–47.
[3] R.L. Hardy, Theory and applications of the multiquadrics—biharmonic method (20 years of discovery 1968–1988), Computers and Mathematics with Applications 19 (1990) 163–208.
[4] J.P. Agnantiaris, D. Polyzos, D.E. Beskos, Some studies on dual reciprocity BEM for elastodynamic analysis, Computational Mechanics 17 (1996) 270–277.
[5] R. Schaback, Error estimates and condition numbers for radial basis function interpolation, Advances in Computational Mathematics 3 (1995) 251–264.
[6] M.J.D. Powell, The uniform convergence of thin plate splines in two dimensions, Numerische Mathematik 68 (1) (1994) 107–128.
[7] E.J. Kansa, A scattered data approximation scheme with application to computational fluid-dynamics—I and II, Computers and Mathematics with Applications 19 (1990) 127–161.
[8] G.E. Fasshauer, Solving partial differential equations by collocation with radial basis functions, in: A.L. Mehaute, C. Rabut, L.L. Schumaker (Eds.), Surface Fitting and Multiresolution Methods, 1997, pp. 131–138.
[9] H. Wendland, Meshless Galerkin method using radial basis functions, Mathematics of Computation 68 (228) (1999) 1521–1531.
[10] M.A. Golberg, C.S. Chen, H. Bowman, Some recent results and proposals for the use of radial basis functions in the BEM, Engineering Analysis with Boundary Elements 23 (1999) 285–296.
[11] C.J. Coleman, On the use of radial basis functions in the solution of elliptic boundary value problems, Computational Mechanics 17 (1996) 418–422.
[12] X. Zhang, K.Z. Song, M.W. Lu, et al., Meshless methods based on collocation with radial basis functions, Computational Mechanics 26 (4) (2000) 333–343.
[13] R. Franke, Scattered data interpolation: test of some methods, Mathematics of Computation 38 (157) (1982) 181–200.
[14] S. Rippa, An algorithm for selecting a good value for the parameter c in radial basis function interpolation, Advances in Computational Mathematics 11 (1999) 193–210.
[15] R.E. Carlson, T.A. Foley, The parameter R^2 in multiquadric interpolation, Computers and Mathematics with Applications 21 (1991) 29–42.
[16] M.A. Golberg, C.S. Chen, S.R. Karur, Improved multiquadric approximation for partial differential equations, Engineering Analysis with Boundary Elements 18 (1996) 9–17.
[17] M.A. Golberg, C.S. Chen, H. Bowman, H. Power, Some comments on the use of radial basis functions in the dual reciprocity method, Computational Mechanics 21 (1998) 141–148.
[18] W.R. Madych, S.A. Nelson, Bounds on multivariate polynomials and exponential error-estimates for multiquadric interpolation, Journal of Approximation Theory 70 (1) (1992) 94–114.
[19] M.J.D. Powell, The theory of radial basis function approximation in 1990, in: F.W. Light (Ed.), Advances in Numerical Analysis, 1992, pp. 105–203.
[20] M.J.D. Powell, A review of algorithms for thin plate spline interpolation in two dimensions, in: F. Fontanella, K. Jetter, P.J. Laurent (Eds.), Advanced Topics in Multivariate Approximations, 1996, pp. 303–322.
[21] W. Light, H. Wayne, Error estimates for approximation by radial basis functions, in: S.P. Singh (Ed.), Approximation Theory, Wavelets and Applications, 1995, pp. 215–246.
[22] S.P. Timoshenko, J.N. Goodier, Theory of Elasticity, third ed., McGraw-Hill, New York, 1970.